MAGNETIC PARTICLES

Ever since the development of the magnetic compass revolutionized navigation in the second century C.E., applications of magnetic materials have become essential in most branches of engineering. In many of these applications the magnetic materials are utilized in the form of microscopic magnetic particles. Some modern representative examples from electrical and electronics engineering are nonvolatile storage of information on magnetic tapes and disks, magnetic inks, refrigerators that make use of the magnetocaloric effect, ferrofluid vacuum seals, and the microscopic machines known as microelectromechanical systems (MEMS). It is likely that these current and emergent engineering applications of microscopic and nanoscopic magnetic particles will be joined by many more in the next few decades.

Even though magnetic particles have been used for a very long time, our understanding of their physical behaviors is relatively new and still limited. In addition, the current understanding of the physical properties of magnetic particles, and the engineering applications that are made possible by these properties, cannot easily be described without sophisticated mathematics. Some of the reasons for this are as follows:

1. The magnetism of magnetic particles is fundamentally quantum-mechanical in origin. Hence, understanding the properties of magnetic particles requires the use of quantum mechanics, either directly or by the inclusion of quantum-mechanical effects into phenomenological models.
2. Magnetism involves vector quantities, which have a direction as well as a magnitude. The magnetic field $\boldsymbol{H}$ (given in units of amperes per meter, A/m), the magnetic moment per unit volume of a magnetic substance $\boldsymbol{M}$ (given in units of A/m), and the magnetic induction or magnetic flux density $\boldsymbol{B}$ (given in units of webers per square meter, Wb/m^2, or tesla, T) are all vector quantities, and their interrelationships must be expressed in terms of vector and tensor equations.
3. For ferromagnetic particles, which are the ones used in most engineering applications, the relationships between the three vector fields $\boldsymbol{H}$, $\boldsymbol{M}$, and $\boldsymbol{B}$ depend on the history of the particle—how the field and magnetization have varied in the past, and possibly how the particle was manufactured.
4. Engineering applications of magnetic particles are determined by physical properties that depend on energy considerations that originate from a number of different physical mechanisms. For example, in spherical particles the coercive field (defined later) is due primarily to the energy associated with crystalline anisotropy, whereas in elongated needlelike single-domain particles the dipole-dipole interactions (the magnetostatic energy) are the most important in determining the coercive field.

Commonly these complications are what make magnetic particles so useful in engineering applications. For example, the dependence of $\boldsymbol{M}$ on the detailed history of the particle is what makes magnetic recording possible.

Most engineering applications utilize large numbers of magnetic particles, which may differ in size, orientation, composition, and so on. However, a detailed understanding of the behavior of such an assortment of particles requires knowledge of the properties of individual particles. The properties of systems consisting of large numbers of particles can be obtained by an appropriate averaging over the size, orientation, shape, type, and location of individual particles.

This article will focus on single magnetic particles. It is only in very recent years that it has become possible to study the behavior of individual particles experimentally. This is due to the development of better methods to produce well-characterized magnetic particles and to the development of magnetic measurement techniques with resolutions at the nanometer scale. These ultrahigh resolution techniques include magnetic force microscopy (MFM) (1), micro-SQUID devices (2), Lorentz transmission electron microscopy (3), and giant magnetoresistive (GMR) measurements (4). These experimental advances are complemented by the emergence of computational science and engineering techniques, such as micromagnetic and Monte Carlo simulations, which allow detailed comparisons between the predictions of models for magnetic particles and experimental data. In this article both high-resolution experimental data for single particles and numerical results from model simulations will be used in the figures to illustrate the physical phenomena described.

TYPES OF MAGNETIC MATERIALS

At the atomic level, a magnetic material is an arrangement of local magnetic moments. Fundamentally, each such magnetic moment is a quantum-mechanical quantity arising from either the intrinsic spin or the orbital motions of the electrons of an atom or molecule. Each of these localized magnetic moments, often simply called "spins" for brevity, may be thought of as a small bar magnet. The microscopic structures of the most widely studied types of magnetic materials are shown schematically in Fig. 1. This figure shows the lowest-energy arrangement (the ground state) of the local magnetic moments or spins in (a) ferromagnetic, (b) antiferromagnetic, and (c) ferrimagnetic materials. The total magnetizations due to the spin arrangements shown in Fig. 1 can be found by adding the vectors together. In a ferromagnet the spins add up to a large vector. For an antiferromagnet they add up to zero. For a ferrimagnet there is some cancellation, but the spins still add up to a nonzero value.

The alignment of the spins in Figs. 1(a) to 1(c) corresponds to a temperature of absolute zero. At nonzero temperatures, the alignment of the spins is somewhat random due to thermal fluctuations. At temperatures above a critical temperature, T_c (which is different for different materials), the thermal fluctuations are so large that the spin arrangement becomes essentially random, the total magnetization is zero, and the material becomes paramagnetic [as shown in Fig. 1(d)]. For ferromagnets in zero applied magnetic field the magnetization vanishes at T_c and remains zero above T_c. Since most engineering applications of magnetic materials use ferromagnets, the remainder of this article will focus on ferromagnetic particles.

RELATIONSHIPS BETWEEN THE VECTOR FIELDS

The fundamental relationship between the vector fields in SI units is given by

$$\boldsymbol{B} = \mu_0(\boldsymbol{H} + \boldsymbol{M}) \tag{1}$$

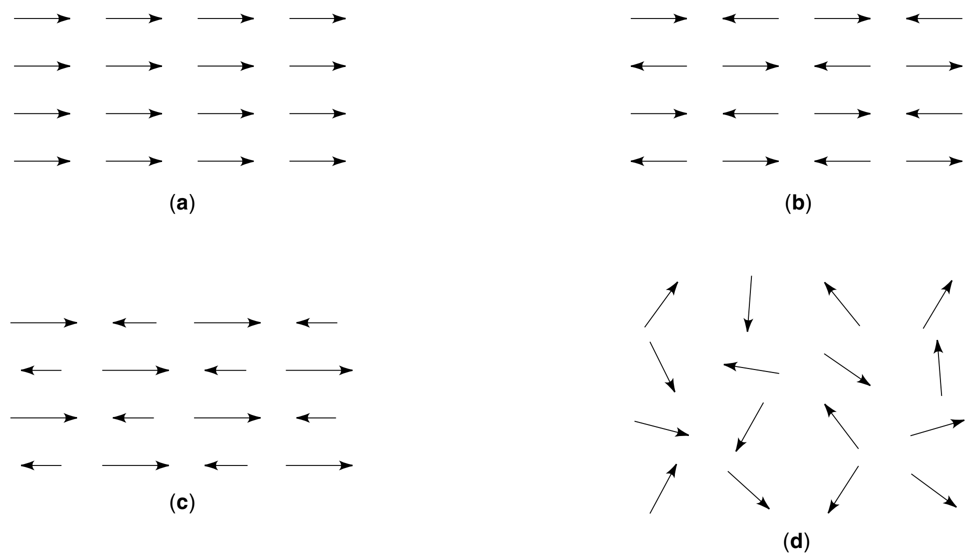

Figure 1. Schematic representation of the arrangement of local magnetic moments or spins in different types of magnetic materials. In (a) all the spins are aligned, and the material is a ferromagnet. The total magnetization, given by the sum of all the spin vectors, is large. In (b) the nearest-neighbor spins are all antialigned, so the total magnetization is zero. This arrangement is that of an antiferromagnetic material. In (c) the nearest-neighbor spins are also antialigned, but here the spins on each sublattice have different lengths. Hence the total magnetic moment is nonzero in this ferrimagnetic material. In (d) the directions of the spins are randomly distributed due to thermal fluctuations so that the total magnetic moment is zero in zero field. This represents a paramagnet. Above a critical temperature, T_c (which is different for different materials), all magnetic materials become paramagnetic.

where $\mu_0 = 4\pi \times 10^{-7}$ H/m (henry per meter) is the permeability of free space. Equation (1) is true for all materials, even for nonlinear ones.

For a linear, homogeneous and isotropic material, the relationship between $\boldsymbol{M}$ and $\boldsymbol{H}$ is linear and given by

$$\boldsymbol{M} = \chi_m \boldsymbol{H} \tag{2}$$

where χ_m is a material-dependent quantity called the magnetic susceptibility. In this case it is possible to write

$$\boldsymbol{B} = \mu_0[1 + \chi_m]\boldsymbol{H} = \mu_0\mu_r\boldsymbol{H} = \mu\boldsymbol{H} \tag{3}$$

where μ is the permeability of the medium and the parameter μ_r is its relative permeability.

In ferromagnetic materials, however, the relationship between the three vector fields is generally nonlinear and history dependent. Thus simple relationships such as those of Eq. (2) and Eq. (3) are not justified. In this case it is necessary to talk about a hysteresis loop (5,6). Figure 2 shows a hysteresis loop, with identification of the intrinsic coercive field H_c, the remanent (spontaneous) magnetization M_r, and the saturation magnetization M_s (the maximum magnetization of a magnetic particle in a strong field). The area of the hysteresis loop corresponds to the work that must be done in taking the magnetic material through one cycle of the applied field. This work is converted to heat and represents a major source of energy loss in devices such as transformers and motors. It was first studied systematically by Ewing, Warburg, and Steinmetz (6) over a century ago. The hysteresis loop shown in Fig. 2 is a nonidealized loop for a small magnetic particle at finite temperature, obtained from a computer simulation of a model magnetic system. Thermal fluctuations in experimental hysteresis loops of nanoscale magnetic particles have been seen in many studies, and they necessitate a probabilistic interpretation of quantities such as the intrinsic coercive field (1,2). Such hysteresis loops indicate that magnetic particles may find applications as nonlinear network elements with intrinsic noise.

One useful classification of magnetic materials for engineering purposes is into soft and hard magnets. Soft magnetic materials are usually used for cores of transformers, generators, and motors, and the heads in magnetic tape and disk devices; applications that require a low coercive field, H_c, small hysteresis loop area to minimize heat generation, or high permeability. Hard magnetic materials are used for electric sensors, loudspeakers, electric meters, magnetic recording media, and other uses that require a high coercive field, a high remanence, or a large hysteresis loss.

Not all hysteresis loops have the shape shown in Fig. 2. In fact, for single-crystal ferromagnets the shape of the hysteresis loop is usually dependent on the orientation of the applied field with respect to the crystalline axes. For materials composed of many different magnetic particles or grains, the nonlinear effects of each particle must be added to obtain a composite hysteresis loop. For such composite materials, or for bulk materials with impurities, the hysteresis loop is not smooth but contains small jumps, called Barkhausen jumps, that correspond to successive switching of small regions of the material (7). These loops can sometimes be parameterized using a model called the Preisach model (8).

MAGNETIC ENERGIES

The energies that are relevant to the properties of magnetic materials arise from a variety of physical effects. Which ones are most important for a particular engineering application depend on the composition of the particular piece of material, its mesoscopic structure (grain size, local stress, etc.), its surface properties, and its size and shape.

Exchange Energy

The exchange energy comes from the quantum-mechanical overlap and hybridization of the exchange integrals between atoms and molecules. Since the interaction constant J is due to the overlap of orbitals, it is a short-range interaction that often does not extend beyond nearest-neighbor pairs of lattice sites. For ferromagnetic materials, Fig. 1(a), $J > 0$, while for antiferromagnetic or ferrimagnetic materials, Fig. 1b(c), $J < 0$. For most materials J is somewhat temperature and stress dependent, due to changes in interatomic distances. It is also dependent on the local environment of a particular magnetic atom. Consequently exchange interactions for atoms at a surface, near a grain boundary, or near an impurity atom may be different from the exchange interaction of the same kind of atom in the bulk of a crystal. Often the Hamiltonian for a magnetic material is written as a sum of Heisenberg terms, such as $\mathcal{H} = J\boldsymbol{S}_i \cdot \boldsymbol{S}_j$, where the three-dimensional spins $\boldsymbol{S}_i$ and $\boldsymbol{S}_j$ are located at nearest-neighbor sites i and j of the crystal lattice.

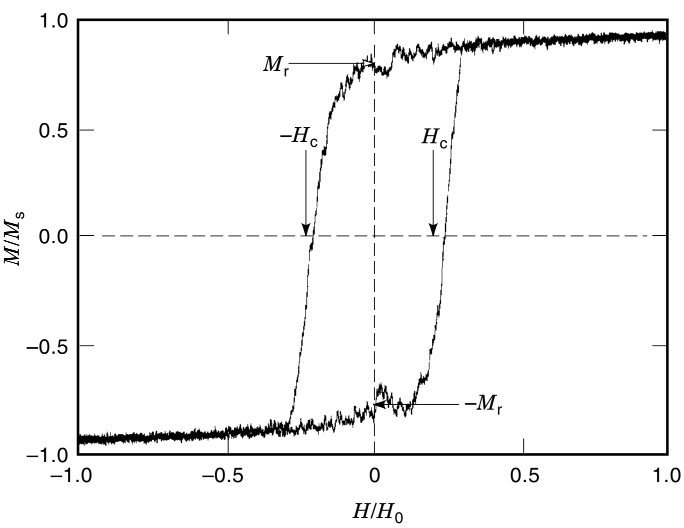

Figure 2. A hysteresis loop for a model of a single-domain uniaxial magnetic particle, the Ising model. An external magnetic field $H_0 \sin(\omega t)$ is applied, and the magnetization is recorded as a function of time. Shown on the loop is the location of the average intrinsic coercive field, H_c. This is the field that must be applied to make the magnetization equal to zero. Also shown is the remanent, or spontaneous, magnetization, M_r. This is the magnetization when the applied field is equal to zero. In this particular model the value of M_r is known exactly. The saturation magnetization, M_s, corresponds to all the spins aligned, as in Fig. 1(a). The fluctuations on the hysteresis loop are due to random thermal noise, which is typically seen in experimental hysteresis loops for small particles at nonzero temperatures as well. This loop is for a temperature of $0.97T_c$. The loop would become smoother at lower temperatures and for larger particles than the 64×64 lattice used here. The loop area can be a complicated function of H_0, ω, and temperature (5). The data used to generate this figure are from a Monte Carlo simulation, courtesy of Dr. Scott W. Sides.

Magnetocrystalline Anisotropy Energy

When magnetic atoms are arranged on a crystal lattice, their spins have a lower energy if they are aligned along certain directions. These are called the easy axes. The directions that require the highest energy for the orientation of the magnetic spins are the hard directions or hard axes. Consequently, certain magnetization directions are preferred. One consequence of magnetocrystalline anisotropy is that hysteresis loops, such as the one shown in Fig. 2, depend on the angles between the applied magnetic field and the crystal axes. In magnetic materials that are not perfect crystals, the orientation of the easy axes in different grains will most likely be different.

For example, iron is a cubic crystal, and the three cube edges are the easy axes. The anisotropy energy of iron is expressed as

$$U_K = K_1(\alpha_1^2\alpha_2^2 + \alpha_2^2\alpha_3^2 + \alpha_3^2\alpha_1^2) + K_2\alpha_1^2\alpha_2^2\alpha_3^2 \quad (4)$$

where the α's are the direction cosines for the angles between the cube edges and the direction of the magnetization. The anisotropy coefficients K_1 and K_2 depend on temperature and are zero above T_c.

Dipole–Dipole Energy

The classical interaction energy between two magnetic dipoles $\boldsymbol{m}_1$ and $\boldsymbol{m}_2$ (which are vector quantities) is given by $U(\boldsymbol{m}_1, \boldsymbol{m}_2) = (\mu_0/4\pi r^3)\,[\boldsymbol{m}_1 \cdot \boldsymbol{m}_2 - 3(\hat{\boldsymbol{r}} \cdot \boldsymbol{m}_1)(\hat{\boldsymbol{r}} \cdot \boldsymbol{m}_2)]$, where $\boldsymbol{r} = r\hat{\boldsymbol{r}}$ is the vector from $\boldsymbol{m}_1$ to $\boldsymbol{m}_2$. This gives a long-range interaction between the dipoles. Since each spin in Fig. 1 represents a magnetic dipole, this dipole-dipole interaction must be considered in dealing with magnetic particles. In many engineering applications where there are no time-varying external fields, the microscopic motion of each individual spin (due to precession and random thermal fluctuations) need not be taken into account, and the familiar equations of magnetostatics are recovered. Consequently, the dipole-dipole interaction is sometimes called the magnetostatic energy. In particular, from magnetostatics the energy stored in the fields is given by

$$U_\mathrm{M} = -\frac{1}{2}\int \boldsymbol{M} \cdot \boldsymbol{H}\,dV \quad (5)$$

where the volume integral is over all ferromagnetic bodies. This may be understood as the integral of the interaction of each dipole with the field $\boldsymbol{H}$ created by all the other magnetic dipoles.

In general, the field inside a uniformly magnetized ferromagnetic body is not uniform, except in very special cases, such as ellipsoids. For an ellipsoid that is uniformly magnetized, the demagnetizing field inside the ellipsoid can be written as $\boldsymbol{H}_\mathrm{d} = -\boldsymbol{NM}$ where $\boldsymbol{N}$ is a tensor. The demagnetizing field is due to the magnetic field caused by all the other dipoles in the particle. When $\boldsymbol{M}$ is parallel to one of the principal axes of the ellipsoid, the tensor is diagonal, and its three diagonal elements are called the demagnetizing factors. Then the magnetostatic self-energy of a uniformly magnetized ellipsoid of volume V is given by

$$U_\mathrm{M} = \frac{V}{2}(N_x M_x^2 + N_y M_y^2 + N_z M_z^2) \quad (6)$$

since the tensor is diagonal. The demagnetizing factors may not be equal, so some directions will be preferred. This gives a shape anisotropy term in the energy of a ferromagnet. Note that the preferred directions from shape anisotropy can be different from the preferred directions for magnetocrystalline anisotropy. For more complicated geometries, a numerical method of solving for $\boldsymbol{H}_d$ and evaluating the integral in Eq. (5) is recommended.

The dipole-dipole interaction is responsible for the formation of magnetic domains. These domains are equilibrium regions where the magnetization is predominantly oriented in a single direction. They are separated by domain walls. Domain walls cost some energy due to the exchange and magnetocrystalline energy terms. However, this energy cost is balanced by the reduction in the magnetostatic energy resulting from the reduction in the total magnetization. Hence large magnetic particles break up into domains magnetized in different directions and separated by domain walls. Domain walls are classified according to the orientation of the spins in the domain-wall region.

For small enough particles the energy cost of a domain wall is always higher than the gain resulting from the reduction in the magnetostatic energy. As a result, sufficiently small particles consist of a single magnetic domain. Nanometer-sized cobalt particles created by electron beam lithography may have only one or a few domains. Figure 3 shows pictures of an array of such particles. Figure 3(a) shows the particles themselves, while Fig. 3(b) shows the magnetic structure of the same particles. Schematic illustrations of the domain structures seen are shown in Figs. 3(c) and 3(d). Even though all of the particles have similar sizes, small differences in their manufacturing histories nevertheless cause their domain structures to be significantly different. This illustrates both the history dependence of magnetic domains and the sensitivity of the magnetization to small changes in the geometry, environment, and composition of a magnetic particle.

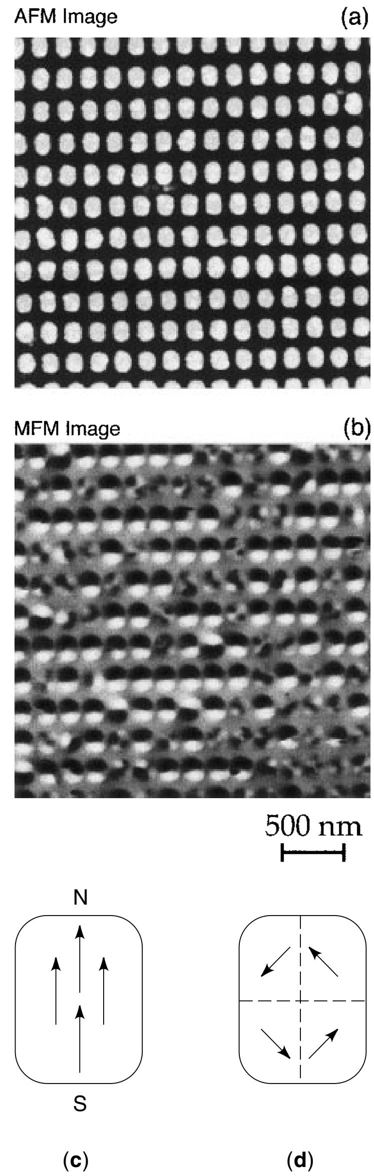

Figure 3. Nanometer-sized magnetic particles of cobalt (Co). These were grown as a polycrystalline film on a GaAs substrate, and electron beam (e-beam) lithography was used to make isolated particles. The substrate in this case should contribute minimally to the magnetization of the particles. The size of these particles is roughly 170 nm, which is about as small as can currently be manufactured using e-beam lithography. Although the particles look uniform, as seen in the atomic force microscope (AFM) image (a), due to the history dependence of magnetic materials different magnetizations are seen in the magnetic force microscope (MFM) image (b). This image measures the magnetic field outside the magnetic particles caused by their individual magnetizations. The dark region corresponds to the north pole and the light region corresponds to the south pole. About two-thirds of the particles are seen to be single domain, while the others have more complicated magnetic arrangements. The domain patterns shown are for the particles as manufactured, before any additional magnetic field was applied. They are schematically illustrated in the sketches (c) and (d). Thanks to Prof. Andrew Kent of the New York University Physics Department for the unpublished AFM and MFM images.

Substrate and Surface Energies

The surface of a magnetic particle can influence its physical behavior as much or even more than the bulk. This is because the energies associated with the exchange interactions and the magnetocrystalline anisotropy are extremely sensitive to the local environment. The environment of a magnetic atom is different at the surface and in the bulk. Surface effects become increasingly important as the particle size is decreased, due to the increased surface-to-volume ratio.

Surface and interface effects can have important engineering applications. For example, GMR materials can be grown by coupling a ferromagnetic film or particle to an antiferromagnetic bulk, leading to an exchange interaction between the interfacial spins of the two types of materials. This gives an exchange bias that leads to an asymmetric hysteresis loop. This is highly desirable because it enhances the signal-to-noise ratio of GMR read heads used in magnetic recording applications.

Surfaces can also affect the response of a magnetic particle to changes in its environment. For example, if the direction of the external field is reversed, reversal of the magnetization of the particle may be initiated at the surface. This can make the coercive field of small particles significantly smaller than it would be in the absence of surfaces.

Magnetostriction and Magnetomechanical Effects

When a magnetic particle is exposed to a magnetic field, its physical dimensions change. This effect, which was discovered in 1842 by Joule, is called magnetostriction. It is related to magnetocrystalline anisotropy and both effects are mainly due to quantum-mechanical spin-orbit coupling.

The application of stress to a magnetic material results in a strain response. The sensitivity of the local magnetization to the local environment means that strain in the lattice will change the local energies (the exchange energy, the magnetocrystalline anisotropy energy, and the dipole–dipole energy), which can alter the behavior of the magnetization locally. This is the inverse magnetostriction effect, commonly called the magnetomechanical effect.

The application of an oscillating magnetic field causes an oscillatory change in the linear dimensions of a magnetic material, which can produce sound waves in surrounding materials. One application of this effect is in magnetostrictive transducers, with uses in sonar, medical technology, and ultrasonic cleaning. The humming sound from electrical transformers is also mainly generated by magnetostriction in the magnetic particles that make up the core.

Temperature

The energy scales associated with the effects discussed previously must be compared with the thermal energy $k_B T$, which causes the randomness of the spins seen in Fig. 1(d). Here k_B is Boltzmann's constant, and the temperature T is given in kelvins. If the thermal energy is comparable to the other energies, it can affect engineering applications. For instance, at nonzero temperature there is some probability that the orientation of the magnetization of a particle will change spontaneously. This can lead to loss of data integrity in magnetic recording media (9).

DYNAMICS OF MAGNETIC PARTICLES

The magnetization dynamics of magnetic particles are important for engineering applications. For example, consider a bit of information to be stored on one of the single-domain particles shown in Fig. 3. The coding may be that a north–south orientation corresponds to Boolean 0 and a south-north orientation to Boolean 1. Engineering questions involving the magnetization dynamics include the following: (1) How strong a field must be applied to change a 0 to a 1 or vice versa? (2) How long can a particle encoded with a bit be exposed to a stray field without losing data integrity, and how strong a stray field can be tolerated? (3) If a bit is written today, how long can it be trusted to remain as it was written?

Metastability

Arguably the most important concept needed to understand the dynamics of magnetic particles is metastability. One familiar example of this ubiquitous natural phenomenon is the supercooling of water. That metastability should be relevant to magnetism is suggested by the fact that the magnetization $\boldsymbol{M}$ of a magnetic particle is history dependent.

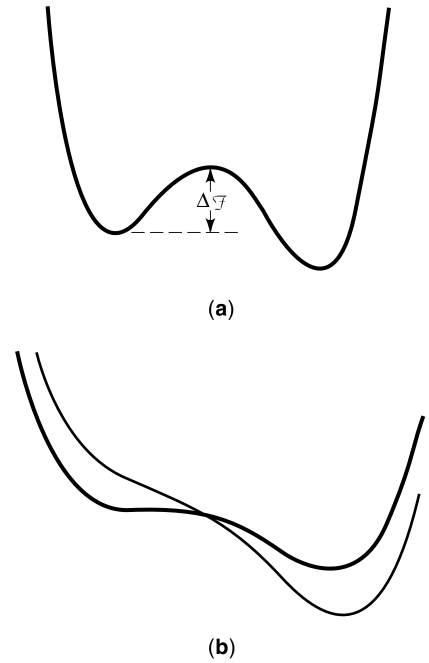

Figure 4. A metastable well is illustrated in (a). Even though the lowest-energy state is on the right, an energy barrier $\Delta\mathscr{F}$ must be overcome before the metastable state on the left can decay to the equilibrium state. As the external magnetic field is increased, the barrier decreases, and it becomes zero at a particular field called the nucleation field, H_{nucl}, as illustrated by the heavy curve in (b). There is no metastable state for higher fields, as illustrated by the light curve in (b).

Figure 4(a) shows the standard picture of metastability in a bistable system, such as a uniaxial single-domain magnetic particle. There are two free-energy minima, one of which is only a local minimum (the metastable state) and one of which is the global minimum (the equilibrium state). If the system is in the metastable state, a free-energy barrier, $\Delta\mathscr{F}$, must be overcome before the system can relax to the equilibrium state. The average lifetime of the metastable state, τ, is given by

$$\tau = \tau_0 \exp\left(\frac{\Delta\mathscr{F}}{k_B T}\right) \tag{7}$$

where τ_0 is an inverse attempt frequency. In magnetic particles τ_0 is typically taken to be on the order of an inverse phonon frequency, usually $\tau_0 \approx 10^{-10}$ s. More detailed analysis shows that τ_0 depends on the curvature of the free energy at both the metastable minimum and the saddle point (the maximum that separates the metastable and equilibrium states).

Once the system has been prepared in the metastable state, how can it get out? There are two possible answers to this question. An analogy is a pitcher half filled with water, which is held above a sink. The water is the system, the pitcher is the metastable state, and the sink is the equilibrium state. One way to get the water into the sink is to shake the pitcher to make the water splash out. The more vigorously the pitcher is shaken, the faster the water will splash out. This method of escape from a metastable state is analogous to a magnetic material at a nonzero temperature. As seen from Eq. (7), the lifetime increases as the height of the barrier increases, whereas it decreases as the temperature increases. Another way of getting the water into the sink is to tip the pitcher. As the pitcher continues to tip, at some point the water starts to flow out. This corresponds to a way of escaping from the metastable state of a magnetic particle, which is valid even at zero temperature. In particular, the barrier $\Delta\mathscr{F}$ depends on the applied field $\boldsymbol{H}_{\text{appl}}$, and changing $\boldsymbol{H}_{\text{appl}}$ corresponds to tipping the pitcher. At a particular value of the field $\Delta\mathscr{F}$ equals zero, and the metastable state disappears. This situation is illustrated in Fig. 4(b). The field that must be applied for $\Delta\mathscr{F}$ to vanish is often called the nucleation field, H_{nucl}.

This pitcher analogy also illustrates an important consideration concerning the escape from a multidimensional metastable well at zero temperature. In particular, how far the pitcher must be tipped before the water starts to spill out depends on the direction in which it is tipped. The smallest angle is needed if the pitcher is tipped to make the water spill from the spout—the lowest part of the rim. Similarly, the nucleation field, H_{nucl}, often depends on the direction of the applied field. However, for thermally driven escape the decay always proceeds across the saddle point (analogous to the spout) as the temperature (analogous to the amplitude of the shaking) is increased, or as the waiting time is increased at fixed temperature.

The waiting time is related to another physical quantity of interest, the probability that a magnetic particle starting in the metastable state at $t = 0$ has never left it at time t. This probability is often called $P_{\text{not}}(t)$. It is only in the last decade that it has become possible to measure $P_{\text{not}}(t)$ for individual single-domain magnetic particles (1,2). For thermal escape over a single barrier one has

$$P_{\text{not}}(t) = \exp(-t/\tau) \tag{8}$$

where τ is given by Eq. (7).

Equation (7) is the fundamental equation needed to understand the dynamics of a magnetic particle. All one requires is a knowledge of $\Delta\mathscr{F}$. This, however, requires a knowledge of the energy of the spin configuration at the saddle point. Since $\Delta\mathscr{F}$ enters in an exponential, the value of τ is extremely sensitive to small changes in $\Delta\mathscr{F}$.

Coherent Rotation

Consider a spherical single-domain uniaxial magnetic particle with magnetocrystalline anisotropy coefficient K and a uniform magnetization $\boldsymbol{M}$ in an applied magnetic field along the easy axis. If all the spins in the particle point in the same direction, the total energy is $E = KV\sin^2(\theta) - M_sVH\cos(\theta)$. Here the saturation magnetization M_s makes an angle θ with the easy axis, and the volume of the particle is V. In this case it is possible to obtain the zero-temperature free-energy barrier exactly—namely,

$$\Delta\mathscr{F} = KV\left[1 + \left(\frac{HM_s}{2K}\right)^2\right]$$

In this model all the spins rotate coherently and act like one large spin. Consequently, particles that behave this way are called superparamagnetic particles. Note that the zero-temperature energy barrier has been assumed to be valid at finite temperatures in this model of a superparamagnet. Since superparamagnetism implies escape over a single barrier, $P_{\text{not}}(t)$ is given by Eq. (8).

The particle volume V enters the metastable lifetime in an exponential, so a small change in particle size can lead to extremely large changes in τ. For example, for an iron sphere with a radius of 115 Å the lifetime $\tau \approx 0.07$ s. If the radius is 140 Å then $\tau \approx 1.5 \times 10^5$ s [42 hours] (10).

The coherent rotation mode described here is often called the Néel–Brown reversal mode (10) since Néel derived Eq. (7) with $\Delta\mathscr{F} = KV/k_BT$ and Brown wrote a differential equation for a random walk in the metastable well to obtain a nonconstant prefactor for Eq. (7). It is also possible to obtain a zero-temperature hysteresis curve using the same assumptions—namely, a uniform magnetization and that only the external field and a uniaxial anisotropy are important. This is called the Stoner–Wohlfarth model (10). This model gives an upper bound for the intrinsic coercive field as $H_c \le 2K/M_s$.

An equivalent analysis for the case in which shape anisotropy is important can also be performed. Again, with the assumption that all the spins always point in the same direction, the analysis is the same except that K now arises from shape anisotropy. The assumption that the spin configuration at the saddle point has all spins pointing in the same direction is only sometimes valid. There are other zero-temperature reversal modes where the zero-temperature saddle point has spins in other configurations. Examples include modes descriptively named buckling, curling, and fanning. The dominant mode depends on the geometry and size of the magnetic particle.

Nucleation and Growth

As the volume V increases, the average rate for magnetization reversal via coherent rotation quickly becomes too small to be practically important. This was illustrated by the example with iron particles discussed previously. Other reversal modes with lower free-energy barriers can then come into play, especially for highly anisotropic materials, in which domain walls are relatively thin.

At nonzero temperatures, thermal fluctuations continually create and destroy small "droplets" of spins aligned with the applied field. The free energy of such a droplet consists of two competing parts: a positive part due to the interface between the droplet and the metastable background, and a negative part due to the alignment of the spins in the droplet with the field. For a droplet of radius R, these terms are proportional to R^{d-1} and $-|H|R^d$, respectively. Here d is the spatial dimension of the particle, and these relations hold both for three-dimensional particles ($d = 3$) and for particles made from a thin film ($d = 2$). Small droplets most likely shrink. However, if a droplet manages to become larger than a critical radius, $R_c \propto 1/|H|$, it will most likely continue to grow and eventually bring the whole particle into the stable magnetization state. The free-energy barrier associated with such a critical droplet is proportional to $1/|H|^{d-1}$, which is *independent* of the particle size! Since the droplets can only grow at a finite speed, in sufficiently large particles or for sufficiently strong fields, new critical droplets may nucleate at different positions while the first droplets formed are still growing.

This droplet switching mechanism gives rise to three regimes of field strengths and particle sizes:

1. For sufficiently weak fields and/or small particles, a critical droplet would be larger than the entire particle. As a result, the saddle point configuration consists of an interface that cuts across the particle, so that $\Delta\mathcal{F} \propto V^{(d-1)/d}$, independent of $|H|$ to lowest order. The behavior in this regime is effectively superparamagnetic, even though the dependence of $\Delta\mathcal{F}$ on the particle size is somewhat weaker than predicted for uniform rotation. In this regime both Eqs. (7) and (8) are valid.
2. For stronger fields and/or larger particles, the magnetization reverses by the action of a single droplet of the stable phase. The free-energy barrier is independent of the particle volume, but because the droplet can nucleate anywhere in the particle, the average lifetime is inversely proportional to V. We call this decay regime the single-droplet regime. A series of snapshots of a computer simulation of single-droplet decay is shown in Fig. 5. In this regime Eq. (8) is still valid.
3. For yet stronger fields and/or larger particles, the decay occurs via a large number of nucleating and growing droplets. In this regime, which we call the multidroplet regime, the average lifetime is independent of V. A series of snapshots of a computer simulation of multidroplet decay is shown in Fig. 6. In this regime Eq. (8) is no longer valid, and $P_{not}(t)$ takes the form of an error function (11,12).

Switching Fields

Two rather similar quantities that are often measured for magnetic particles are the switching field, H_{sw}, and the intrinsic coercive field, H_c. The former is defined as the magnitude of the field for which a particle switches with probability 1/2 within a given waiting time after field reversal. The latter is the value of the field at which the magnetization crosses the field axis, as shown in the hysteresis loop in Fig. 2. Both depend weakly on the time scale of the experiment (waiting time or field cycle time), but they are qualitatively similar over a wide range of time scales. A collection of experimentally measured coercive fields for various materials are shown as functions of particle size in Fig. 7(a) (11). The increase in H_c with particle size for small sizes is due to the superparamagnetic behavior of the particles, whereas the decrease for larger sizes is due to the dipole-dipole interaction, which causes large particles to break up into multiple domains. For particles in the nanometer range, which are single-domain in equilibrium, the crossovers between the three nucleation driven magnetization reversal mechanisms described previously give rise to very similar size dependences (12,13), as seen from the computer simulation data in Fig. 7(b).

Domain Boundary Movement

If the magnetic particle is multidomain in zero field, the application of a magnetic field will cause the domain wall(s) to move. In this case the dynamics of the magnetization are dominated by the domain-wall movement. Typically there will be pinning sites due to impurities, grains, and surfaces that the domain wall must overcome before it can move. These obstacles can either be overcome by applying a sufficiently large field or by waiting for random thermal fluctuations to move the domain wall past the pinning centers. This is analogous to the zero-temperature and finite-temperature reversal mechanisms in single-domain particles. If the domain wall moves due to random thermal fluctuations, the magnetization of the particle will change slowly with time, a phenomenon called magnetization creep (13).

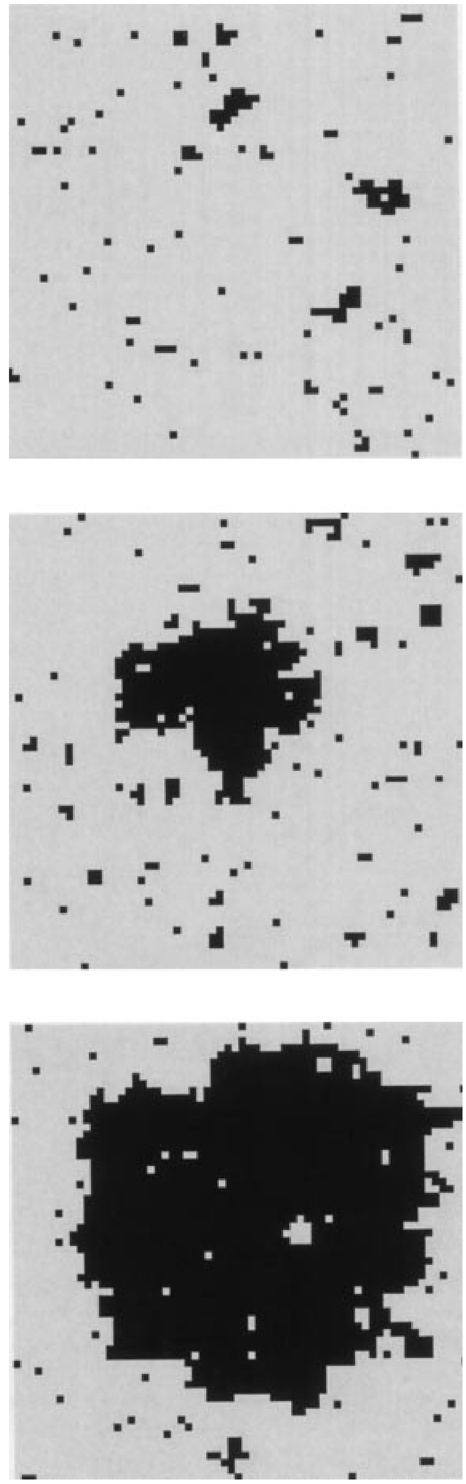

Figure 5. Three snapshots from a computer simulation of the single-droplet switching mechanism for a model of a particle made from a highly anisotropic, uniaxial ultrathin magnetic film. Time increases from top to bottom in the figure. Data courtesy of Dr. György Korniss.

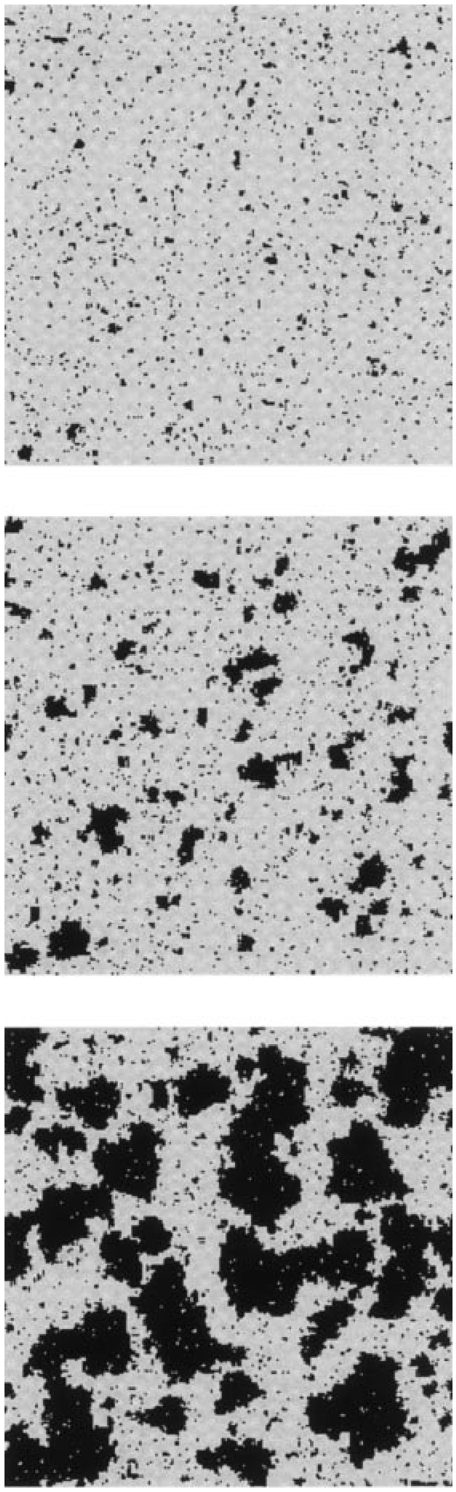

Figure 6. Three snapshots from a computer simulation of the multi-droplet switching mechanism for a model of a particle made from a highly anisotropic, uniaxial ultrathin magnetic film. Time increases from top to bottom in the figure. Data courtesy of Dr. György Korniss.

Magnetic Viscosity

Consider a large number of identical noninteracting particles. If a strong field is applied and then quickly removed, the remanent magnetization will decay with time as $M_r(t) = M_r(0)\exp(-t/\tau)$ as particles cross the barrier separating the two equilibrium states. However, in the typical case the particles are not identical, and there is a distribution of lifetimes, $\mathscr{P}(\tau)$. In this case the time decay is

$$M_r(t) = M_r(0)\int_0^\infty \mathscr{P}(\tau)\exp(-t/\tau)\,d\tau \tag{9}$$

Under some circumstances and for certain specific distribu-

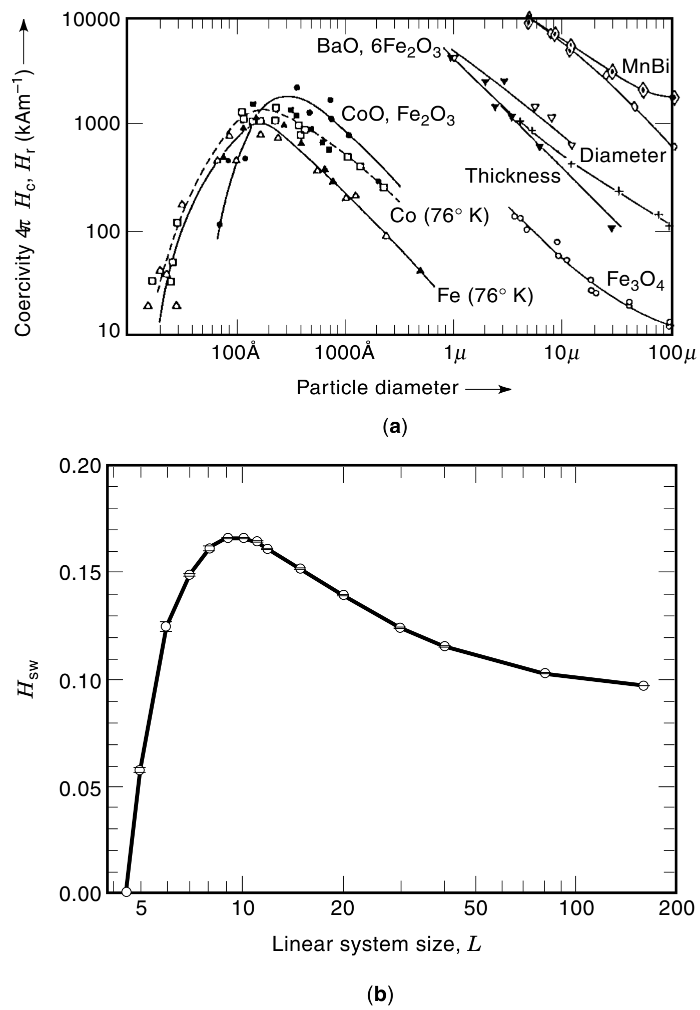

Figure 7. Plots of the intrinsic coercive and switching fields versus particle size. As explained in the text, these fields can be considered to be roughly the same. (a) The intrinsic coercive field, H_c, for magnetic particles of various materials, shown versus the particle diameter. Reproduced from (11) with permission from John Wiley & Sons, Ltd. (b) For a simple model for a uniaxial single-domain particle, the $L \times L$ two-dimensional Ising model, simulations show a maximum in H_{sw} (in units of J) versus L, even when there are no dipole-dipole interactions so that particles of all sizes remain single domain. This effect is due to different nucleation decay mechanisms for particles of different size (12,13), as described in the text.

tions $\mathscr{P}(\tau)$, Eq. (9) can be approximated by $M_r(t) \approx C - S \ln(t/\bar{t}_0)$, where C, S, and $\bar{t}_0$ are constants. This logarithmic decay of the magnetization is called magnetic viscosity. It must be emphasized that this logarithmic equation is a valid approximation *only* under certain specific circumstances and even then *only* for a limited range of t (10).

MAGNETOCALORIC EFFECTS

Magnetocaloric effects of magnetic particles have engineering applications principally in refrigeration. Current applications are mostly in ultralow temperature refrigeration below a few kelvins, but near-term applications close to room temperature seem promising. Given that at constant volume the $P\ dV$ work term is zero, the first law of thermodynamics becomes

$$đQ = dU - đw = dU - \mu_0 \boldsymbol{H} \cdot đ\boldsymbol{M} \tag{10}$$

where U is the internal energy of the magnetic particle, and Q and w represent heat and magnetic work, respectively. The symbol $đ$ denotes an infinitesimal change rather than a true differential. This must be considered because of the history dependence of $\boldsymbol{M}$. For an adiabatic change, $đQ = TdS = 0$, where S is the entropy. Then the relation

$$\Delta T = -\frac{T}{C_{\mathrm{H}}} \left(\frac{\partial M}{\partial T} \right)_{\mathrm{H}} \Delta H \tag{11}$$

can be obtained (14), where C_{H} is the heat capacity at constant field. Thus an increase in H produces a rise in temperature, and vice versa, which is the magnetocaloric effect. This can be utilized as a cooling mechanism by placing the magnetic material in a strong applied field and then turning off the applied field. This will lead to a decrease in temperature due to adiabatic demagnetization according to Eq. (11).

ACKNOWLEDGMENTS

This work was supported by the US National Science Foundation Grants No. DMR-9520325 and DMR-9871455, and by Florida State University through the Center for Materials Research and Technology, the Supercomputer Computations Research Institute (US Department of Energy Contract No. DE-FC05-85ER25000), and the Department of Physics. Supercomputer time at the National Energy Research Supercomputer Center was provided by the US Department of Energy.

BIBLIOGRAPHY

1. M. Lederman, S. Schultz, and M. Ozaki, Measurement of the dynamics of the magnetization reversal in individual single-domain ferromagnetic particles, *Phys. Rev. Lett.,* **73**: 1986–1989, 1994.
2. W. Wernsdorfer et al., Experimental evidence of the Néel-Brown model of magnetization reversal, *Phys. Rev. Lett.,* **78**: 1791–1794, 1997.
3. C. Salling et al., Measuring the coercivity of individual sub-micron ferromagnetic particles by Lorentz microscopy, *IEEE Trans. Magn.,* **27**: 5184–5186, 1991; C. Salling et al., Investigation of the magnetization reversal mode for individual ellipsoidal single-domain particles of γ-Fe_2O_3, *J. Appl. Phys.,* **75**: 7989–7992, 1994.
4. V. Cros et al., Detection of the magnetization reversal in submicron Co particles by GMR measurements, *J. Magn. Magn. Mater.,* **165**: 512–515, 1997.
5. S. W. Sides, P. A. Rikvold, and M. A. Novotny, *J. Appl. Phys.,* **83**: 6494–6496, 1998.
6. J. A. Ewing and C. P. Steinmetz, On effects of retentiveness in the magnetization of iron and steel, *Proc. Roy. Soc. (London),* **34**: 39–45, 1882; E. Warburg, Magnetische Untersuchungen, *Ann. Phys. Chem. (Neue Folge),* **13**: 141–164, 1882; C. P. Steinmetz, On the law of hysteresis, *Trans. Am. Inst. Electr. Eng.,* **9**: 3–51, 1892.
7. O. Perkovic, K. Dahmen, and J. P. Sethna, Avalanches, Barkhausen noise, and plain old criticality, *Phys. Rev. Lett.,* **75**: 4528–4531, 1995.
8. I. D. Mayergoyz, *Mathematical Models of Hysteresis,* New York: Springer-Verlag, 1991; C. E. Korman and P. Rugkwamsook, Identification of magnetic aftereffect model parameters: comparison of experiment and simulations, *IEEE Trans. Magn.,* **33**: 4176–4178, 1997.
9. T. Yogi and T. A. Nguyen, Ultra high density media: gigabit and beyond, *IEEE Trans. Magn.,* **29**: 307–316, 1993; P. L. Lu and S. Charap, Thermal instability at 10 Gbit/in^2 magnetic recording, *IEEE Trans. Magn.,* **30**: 4230–4232, 1994; I. Klik, Y. D. Yao, and C. R. Chang, Chain formation, thermal relaxation and noise in magnetic recording, *IEEE Trans. Magn.,* **34**: 358–362, 1998; J. J. Lu and H. L. Huang, Switching behavior and noise in obliquely oriented recording media, *IEEE Trans. Magn.,* **34**: 384–386, 1998; E. N. Abarra and T. Suzuki, Thermal stability of narrow track bits in 5 Gbit/in^2 medium, *IEEE Trans. Magn.,* **33**: 2995–2997, 1997; Y. Hosoe et al., Experimental study of thermal decay in high-density magnetic recording media, *IEEE Trans. Magn.,* **33**: 3028–3030, 1997.
10. A. Aharoni, *Introduction to the Theory of Ferromagnetism,* Chap. 5. Oxford: Oxford Univ. Press, 1996.
11. R. S. Tebble and D. J. Craik, *Magnetic Materials,* London: Wiley, 1969.
12. H. L. Richards et al., Magnetization switching in nanoscale ferromagnetic grains: description by a kinetic Ising model, *J. Magn. Magn. Mater.,* **150**: 37–50, 1995.
13. P. A. Rikvold et al., Nucleation theory of magnetization reversal in nanoscale ferromagnets, in A. T. Skjeltorp and D. Sherrington (eds.), *Dynamical Properties of Unconventional Magnetic Systems,* NATO Science Series E: Applied Sciences, Vol. 349, Dordrecht: Kluwer, 1998, pp. 307–316.
14. D. Craik, *Magnetism, Principles and Applications,* , Chap. 1. New York: Wiley, 1995.

Reading List

A. Aharoni, *Introduction to the Theory of Ferromagnetism,* Oxford: Oxford Univ. Press, 1996.

H. N. Bertram, *Theory of Magnetic Recording,* Cambridge, UK: Cambridge Univ. Press, 1994.

S. Chikazumi, *Physics of Magnetism,* Malabar, FL: Krieger, 1978.

D. Craik, *Magnetism, Principles and Applications,* New York: Wiley, 1995.

J. C. Mallinson, *The Foundations of Magnetic Recording,* 2nd ed., Boston: Academic Press, 1993.

For a review of recent experimental studies of magnetization switching in magnetic nanoparticles, see the introduction of H. L. Richards et al., Effects of boundary conditions on magnetization switching in kinetic Ising models of nanoscale ferromagnets, *Phys. Rev. B,* **55**: 11521–11540, 1997.

M. A. Novotny
P. A. Rikvold
Florida State University

MAGNETIC RECORDING. See MAGNETIC TAPE RECORDING.